Granular Matter
DOI 10.1007/s10035-014-0491-7

ORIGINAL PAPER

Grainsize dependence of clastic yielding in unsaturated granular soils

Y. D. Zhang · G. Buscarnera

Received: 10 October 2013

Abstract We use a recent reformulation of the Breakage Mechanics theory explaining comminution in wet granular assemblies. By using a dataset for sands, we quantify the relation between a geometric descriptor of the assembly (i.e., the mean grainsize) and the model constants that control the suction air-entry value and the stress threshold at the onset of crushing. Such relations are used to define two contrasting scenarios for the coupling between degree of saturation and yielding. In the first scenario, the suction air-entry value scales inversely with the mean grainsize, while the energy input for comminution is assumed to be independent of the size of the particles. The outcome of this assumption is that changes in degree of saturation are predicted to play a more intense role in finer gradings. Conversely, if we assume that also the energy input for grain breakage scales inversely with the size of the particles, the effect of the degree of saturation is predicted to be stronger in coarser assemblies. In other words, the deterioration of the yielding stress due to grainsize scaling effects is predicted to exacerbate the water sensitivity of unsaturated crushable soils. This result provides an interpretation for the evidence that solid–fluid interactions have a noticeable role in the compression response of assemblies made of coarse brittle particles (e.g., gravels or rockfill), while they tend to play little or no role in granular materials characterized by a finer grading (e.g., sands).

Keywords Unsaturated soils · Particle breakage · Grainsize effects · Capillary effects · Yielding

Y. D. Zhang · G. Buscarnera (✉)
Department of Civil and Environmental Engineering, Northwestern University, 2145 Sheridan Road, Evanston, IL 60208, USA
e-mail: g-buscarnera@northwestern.edu

1 Introduction

The high-pressure compaction of granular materials is accompanied by comminution [1,2]. As a result, it involves changes in the grain size distribution [3,4] and alterations of hydrologic properties like hydraulic conductivity [5–7] and fluid-retention capability [8–10]. Hydro-mechanical couplings in particulate media are apparent also in other forms. For example, the stress threshold at the onset of plastic strains in unsaturated soils depends on the amount of water stored in the pores [11–13]. In other words, passing from saturated to unsaturated conditions, the yielding threshold tends to shift to larger values, postponing the onset of plastic compaction. Similar effects have been found also in granular compounds prone to comminution, such as rockfill and gravels [14,15], in which particle breakage can be triggered by either external loading or changes in relative humidity [15]. A number of civil and industrial problems interact with these hydro-mechanical processes, including the quantification of the deformations of earth dams [16], the design of infrastructural materials [17] and the production of ceramic and pharmaceutical products [18,19].

Although the interplay between mechanical and hydrologic processes is controlled by interactions at particle scale, usual constitutive models capture hydro-mechanical coupling via phenomenological fits. This strategy supports the solution of engineering problems under specific conditions, but it does not reconcile the macro-scale observations with their microscopic origin, nor emphasizes the role of microstructural attributes (e.g., pore size, particle geometry, etc.). Indeed, unsaturated soil mechanics suggests several cases in which microstructural phenomena control the macroscopic couplings. For example, as far as plastic yielding is concerned, changes in degree of saturation have an important role in fine-grained materials such as clays, pow-

Published online: 04 April 2014

ders and silts[11,20,21], in which suction affects the formation and evolution of micro- and macro-pores [22]. Noticeable effects of solid–fluid interactions have been found also in coarse-grained soils, where the hydraulic effects are controlled by intra-particle fractures [23,24]. By contrast, granular materials with a grainsize intermediate between the two above mentioned end-members (e.g., sands) are controlled by capillary effects due to inter-particle water menisci [25,26]. In this case, experiments have shown that the deformation response of these geomaterials tends to be characterized by minor suction effects, that become negligible when the sand reaches a sufficient density [27].

Research on sands, however, supports the identification of the basic mechanisms and provides opportunities for theoretical studies [28–31]. In fact, suction effects in these materials can be explained via simple capillary interactions [32]. In addition, as in all classes of soils, the compression response of sands is dominated by the interaction among multiple units [31,33], which makes them a very convenient scheme to understand the influence of particle-scale phenomena and hydro-mechanical interactions. Based on these considerations, here we use a recent reformulation of the Breakage Mechanics theory [34,35] for unsaturated granular soils [37]. The most relevant feature of the theory is the ability to account for the statistics of the grainsize distribution, thus enabling particle-scale processes to be incorporated via scaling functions and statistical homogenization [34]. Buscarnera and Einav [37] have linked this approach to the capillary theory, thus providing a connection between solid–fluid interactions, grainsize characteristics and particle comminution. The main goal of the paper is to use the above mentioned theory to investigate the coupling between grainsize properties and macroscopic yielding in unsaturated granular compounds. To pursue this goal, we use a dataset of hydraulic and mechanical properties of granular media. Data and theory are eventually combined, with the purpose to infer the possible grainsize-dependence of the constants that control hydro-mechanical coupling at the macroscale.

2 Unsaturated breakage mechanics

Buscarnera and Einav [37] have studied the mechanics of particle breakage under unsaturated conditions in the frame of continuum thermodynamics [38]. The most notable features of their theory are the use of energy input and thermodynamic potentials expressed as functions of mechanical and hydrologic variables, as well as the incorporation of particle scaling laws inspired by microscopic solid–fluid interactions. More specifically, the work input has been expressed in accordance with the form suggested by Houlsby [28] for unsaturated soils, while the Helmholtz free energy has been assumed to be given by the sum of a strain-energy component and a hydraulic term, both dependent on the evolving grainsize characteristics. The resulting energy potential has been obtained via statistical homogenization [34]:

$$\Psi\left(\varepsilon_{ij}^{e}, S_r, B\right) = \int_{D_m}^{D_M} g\left(B, x\right) \psi\left(\varepsilon_{ij}^{e}, S_r, x\right) dx \tag{1}$$

$$\psi\left(\varepsilon_{ij}^{e}, S_r, x\right) = \psi^{M}\left(\varepsilon_{ij}^{e}, x\right) + \psi^{H}\left(S_r, x\right) \tag{2}$$

where x is the grain size that spans between the minimum and maximum diameters (D_m and D_M); Ψ and ψ are the total and specific grainsize Helmholtz energy potential, respectively; the superscripts M and H correspond to mechanical and hydraulic contributions, respectively; ε_{ij}^{e} indicates the elastic strains of the skeleton; S_r is the degree of saturation; $g(B, x)$ is the probability density function representing the current grainsize distribution (GSD), here expressed as a function of the breakage index B. This index can be seen as a scalar descriptor of the current GSD relative to the initial and ultimate GSDs. Similar to the concept of damage variable D used in continuum damage mechanics, the breakage index B can be considered as a thermodynamic state variable that spans from 0 to 1 to represent the transition from the initial unbroken state to the ultimate comminuted state[34]. According to the theory, the grainsize dependence of the mechanical and hydraulic potentials can be represented by using multiplicative decompositions of the following form:

$$\psi^{K}\left(\varepsilon_{ij}^{e}, S_r, x\right) = \psi_r^{K}\left(\varepsilon_{ij}^{e}, S_r\right) f_K\left(x\right) \tag{3a}$$

$$f_K\left(x\right) = \left(x / D_{rK}\right)^{n_K} \tag{3b}$$

in which ψ_r^K is a reference free energy function, $f_K(x)$ a grainsize scaling function and D_{rK} a reference grainsize. The subscript K in Eq. (3) can coincide either with M (mechanical) or H (hydraulic) and the grainsize scaling laws for each component can be assessed on the basis of micro-scale considerations. For example, mechanical contributions can be defined by recognizing that larger particles statistically store more strain energy due to their larger surface area and the higher frequency of interparticle contacts [34]. To a first order, in the case of spherical particles, this scaling attains quadratic dependence (i.e., $n_M = 2$). Similarly, the hydraulic scaling function $f_H(x)$ can be defined on the basis of solid–fluid interactions at particle scale. Indeed, in presence of capillary interactions exerted by water menisci, the additional forces can be quantified through the capillary theory [32], thus suggesting a scaling law inversely proportional to the grainsize (i.e., $n_H = -1$).

The incorporation of these scaling functions in the statistical homogenization of Eq. (1) generates the following expression of Helmholtz free energy potential

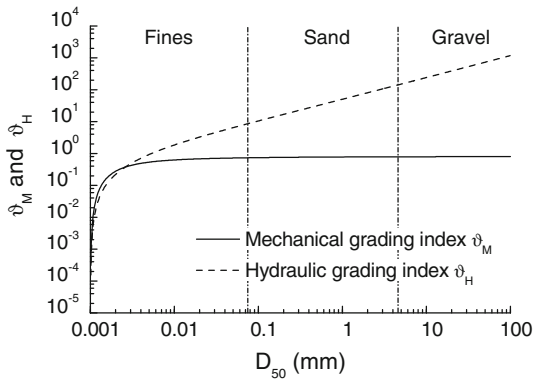

Fig. 1 Grading indices ϑ_M and ϑ_H: dependence on mean particle size D_{50} for a uniform initial GSD (where the minimum particle size, D_m, is assumed to be 1 μ)

$$\Psi\left(\varepsilon_{ij}^{e}, S_r, B\right) = (1-\vartheta_M B)\,\psi_r^M\left(\varepsilon_{ij}^{e}\right) + (1+\vartheta_H B)\,\psi_r^H\left(S_r\right) \tag{4}$$

in which the evolving breakage index B appears in both the mechanical and the hydraulic components. The indices ϑ_M and ϑ_H are geometrical descriptors of the granular assembly and depend on the scaling laws, as well as on initial and ultimate grainsize distributions employed for the definition of B.

Figure 1 illustrates an example of the dependence of these grading indices on the average grainsize for the case of initial uniform grading and ultimate fractal grading (see Appendix A for more details on this procedure).

As shown by Buscarnera and Einav [37], Ziegler's orthogonality principle allows one to define the work-conjugated counterparts of the state variables in Eq. (4), as follows:

$$\sigma'_{ij} = \frac{\partial\Psi}{\partial\varepsilon_{ij}^{e}} = (1-\vartheta_M B)\,\frac{\partial\psi_r^M}{\partial\varepsilon_{ij}^{e}} \tag{5a}$$

$$ns = -\frac{\partial\Psi}{\partial S_r} = -(1+\vartheta_H B)\,\frac{\partial\psi_r^H}{\partial S_r} \tag{5b}$$

$$E_B = -\frac{\partial\Psi}{\partial B} = \vartheta_M\psi_r^M - \vartheta_H\psi_r^H \tag{5c}$$

where $\sigma'_{ij} = \sigma_{ij}^{net} + sS_r\delta_{ij}$ is a generalized effective stress; ns the smeared suction and E_B the *breakage energy*. To complete the framework, it is possible to include contributions associated with plastic processes, such as frictional dissipation and pore collapse [35]. Such effects generate inelastic strain rates, $\dot{\varepsilon}_{ij}^{p}$, that can be incorporated via a coupled expression of the dissipation rate ([35]). In the case of coupling between breakage and frictional dissipation, the yielding condition can be expressed as follows:

$$\frac{E_B}{E_c}(1-B)^2 + \left(\frac{q}{Mp'}\right)^2 \leq 1 \tag{6}$$

where $p' = \frac{1}{3}\sigma'_{ii}$ and $q = \sqrt{3J_2} = \sqrt{\frac{3}{2}s_{ij}s_{ij}}$ are two quantities associated with the first and second stress invariants, respectively, E_c is the energy threshold to initiate particle crushing under isotropic stress conditions and M is the stress ratio at frictional failure. The yielding condition Eq. (6) is written as a function of the breakage energy, E_B. Hence, in analogy with fracture mechanics, the model postulates that crushing is initiated when an energy measure attains a threshold value, here assumed to scale with the constant E_c [36]. As a result, the conditions at the onset of crushing do not depend directly on the hydrologic variables (e.g., ns or S_r), but such dependence is incorporated indirectly via E_B, depending on how this variable is affected by the hydraulic state. Buscarnera and Einav [37] have found that, given the different grainsize scalings of mechanical and hydraulic components of the Helmholtz free energy, deformations and solid–fluid interactions have opposite effects on the breakage energy [see Eq. (5c)]. More specifically, capillary effects reduce the energy available for particle crushing, causing that further elastic deformations are needed to comminute the assembly. Solid–fluid interactions are therefore predicted to generate a further energy barrier that requires additional external loading to compensate the effects of capillarity. In other words, this energy-based approach allows the model to reproduce suction-hardening phenomena without specific phenomenological assumptions at the macroscale. This aspect can be easily shown with reference to isotropic loading conditions (i.e., $q = 0$). From Eqs. (5) and (6), the hydrostatic comminution pressure can indeed be expressed as follows:

$$p'_{CR}\left(S_r, B\right) = p'_{CR_0}\left(B\right)\chi_{HB}\left(S_r, B\right) \tag{7}$$

where p'_{CR_0} indicates the comminution pressure for a fully saturated medium and χ_{HB} is a capillary breakage factor representing the effect of the degree of saturation. Since the size of the elastic domain scales with the magnitude of p'_{CR}, changes in p'_{CR} dictated by fluctuations in S_r imply expansions and/or contractions of the yield surface, possibly being the cause of inelastic processes [37]. Notably, this result derives from the scaling laws used for the energy potentials, thus suggesting that the coupling between degree of saturation and yielding can be seen as a natural outcome of solid–fluid interactions at the micro-scale. These convenient features of the theory, together with the possibility to incorporate data about the grainsize characteristics of the assembly, will be exploited in the following to elucidate the implications of the constitutive assumptions (e.g., elastic and retention models) and the possible existence of grainsize dependencies in the quantities that control hydro-mechanical coupling.

3 Analytical inspection of hydro-mechanical coupling

According to the previous section, an appropriate description of elastic response and retention behavior should rely on suitable energy potentials. Such potentials enter into the expression of the breakage energy [Eq. (5c)], thus affect initial size and evolution of the yielding domain [Eq. (7)]. In this section we explore such dependencies considering different options for the hydro-mechanical energy potentials.

3.1 Elastic models

Linear elasticity (L-E) can be considered as the simplest option for the strain-dependent component of the Helmholtz free energy, and can be expressed in the following form:

$$\psi_r^M\left(\varepsilon_v^e, \varepsilon_s^e\right) = \frac{1}{2}\left(K\varepsilon_v^{e\,2} + 3G\varepsilon_s^{e2}\right) \tag{8}$$

where K and G are the effective bulk and shear modulus, while $\varepsilon_v^e = \varepsilon_{ii}^e$ and $\varepsilon_s^e = \sqrt{\frac{2}{3}e_{ij}e_{ij}}$ indicate volumetric and deviatoric elastic strains. The expression of the yield function in the stress space can be derived by substituting Eqs. (8) and (5) into (6), obtaining:

$$\frac{\vartheta_M}{E_C}\frac{(1-B)^2}{(1-\vartheta_M B)^2}\frac{1}{2}\left(\frac{p'^2}{K}+\frac{q^2}{3G}\right)+\left(\frac{q}{Mp'}\right)^2 \leq 1+\frac{\vartheta_H}{E_C}\psi_r^H\left(S_r\right)(1-B)^2 \tag{9}$$

The two components of the hydrostatic comminution pressure p'_{CR} in Eq. (7) are in this case characterized by the following expressions:

$$p'_{CR_0}(B) = \frac{1-\vartheta_M B}{1-B}\sqrt{\frac{2KE_c}{\vartheta_M}} \tag{10a}$$

$$\chi_{HB}\left(S_r, B\right) = \frac{p'_{CR}}{p'_{CR_0}} = \sqrt{1+\frac{\vartheta_H}{E_c}\psi_r^H\left(S_r\right)(1-B)^2} \tag{10b}$$

Equation (10a) indicates that the stress threshold at the onset of comminution (i.e. $B = 0$) in a saturated medium evolves with B (a process referred to as *clastic hardening*[39]). In addition, Eq. (10b) suggests that the expression of the hydraulic part of the Helmholtz free energy plays a direct role in determining how the breakage strength evolves with S_r.

More sophisticated descriptions of the elastic behavior of granular materials can also be used. A possible option is the pressure-dependent hyperelastic model used by Nguyen and Einav [40] and inspired by the hyperelastic model of Einav and Puzrin [41], in which the Helmholtz free energy potential takes following form:

$$\psi_r^M\left(\varepsilon_v^e, \varepsilon_s^e\right) = \frac{p_r}{\bar{K}(2-m)}\Lambda^{\frac{2-m}{1-m}} + \frac{3}{2}p_r\bar{G}\Lambda^{\frac{m}{1-m}}\varepsilon_s^{e2} \tag{11}$$

where $\Lambda = \bar{K}(1-m)\varepsilon_v^e + 1$, p_r is a reference pressure (here assumed to be equal to 1 kPa), m is a model constant that controls the pressure dependence of the elastic stiffness (for sands typically assumed to be 0.5) and $\bar{K}$ and $\bar{G}$ are non-dimensional elastic constants. Following the same procedure, the two components of the comminution pressure p'_{CR} in Eq. (7) can be derived as follows:

$$p'_{CR_0}(B) = p_r\frac{(1-\vartheta_M B)}{(1-B)^{\frac{2}{2-m}}}\left(\frac{(2-m)\bar{K}E_c}{\vartheta_M p_r}\right)^{\frac{1}{2-m}} \tag{12a}$$

$$\chi_{HB}\left(S_r, B\right) = \left(1+\frac{\vartheta_H}{E_c}\psi_r^H\left(S_r\right)(1-B)^2\right)^{\frac{1}{2-m}} \tag{12b}$$

By comparing Eqs. (10) with (12) it is readily apparent that changes in the main assumptions about the elastic behavior of the assembly have implications also in terms of inelastic characteristics, such as clastic hardening and suction-dependence of the yielding thresholds.

3.2 Water retention models

The hydraulic part of the Helmholtz free energy can be used to reproduce the water-retention response of the granular medium. A simple yet qualitatively efficient model is the hyperbolic retention curve used by Buscarnera and Einav [37], which is characterized by the following relation between degree of saturation and smeared suction:

$$ns = K_w\left(\frac{1}{S_r}-1\right) \tag{13}$$

where K_w is a material constant associated with the suction air-entry value (s_{AEV}) of the medium. A second option explored in the following is inspired by the expression of state surface proposed by Lloret and Alonso [42] and later used by Alonso et al. [11]:

$$ns = K_w\tanh^{-1}\left(1-S_r\right) = \frac{K_w}{2}\ln\left(\frac{2-S_r}{S_r}\right) \tag{14}$$

where K_w controls again s_{AEV}. In the following the function given by Eq. (14) will be referred to as logarithmic retention model. The hydraulic part of the reference Helmholtz free energy function can be obtained by integrating Eqs. (13) and (14) with respect to S_r. For the hyperbolic retention curve, the hydraulic potential takes the form:

$$\psi_r^H\left(S_r\right) = K_w\left(S_r - \ln\left(S_r\right) - 1\right) \tag{15}$$

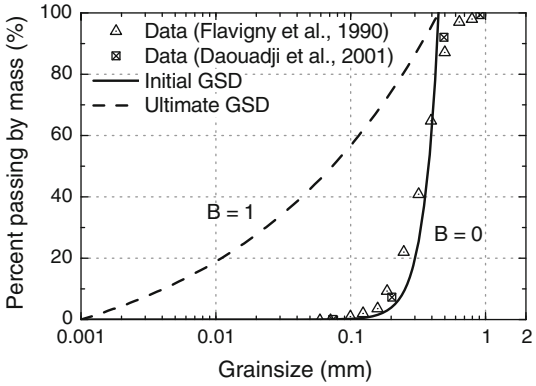

Fig. 2 Grain size distribution (GSD) of Hostun sand. The initial GSD is fitted through a uniform grading; the ultimate GSD is assumed to be given by a power law.

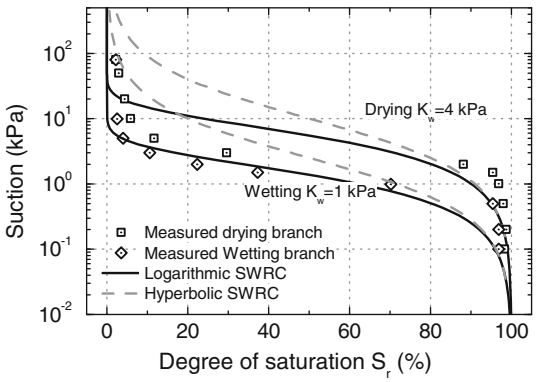

Fig. 3 Calibration of the parameters of the soil water retention curve (SWRC) of Hostun sand

while for the logarithmic retention curve it reads as:

$$\psi_r^H(S_r) = \frac{1}{2} K_w \left(S_r \ln(S_r) + (2 - S_r) \ln(2 - S_r)\right) \qquad (16)$$

The combination of strain-dependent and saturation-dependent potentials eventually defines the characteristics of both clastic yielding and suction-dependent hardening.

3.3 Calibration of model constants and prediction of coupling effects

This section illustrates the strategy for the calibration of the model constants with reference to an extensively tested quartzitic granular material: Hostun sand. Different elasticity and retention models are considered, discussing the effect of the selected models on the predicted characteristics of clastic yielding and suction-hardening. The considered sand is characterized by a uniform grading, as illustrated by the GSDs reported in Fig. 2, which were extracted from two different studies [43,44]. The initial GSD can be fitted by Eq. (22), using a mean grainsize $D_{50} = 0.38$ mm. As a result, the grading indices ϑ_M and ϑ_H are computed according to Eqs. (25a) and (25b) (see Appendix A for more details on the mathematical expression of the initial grainsize distribution). Data on the water retention response of Hostun sand are taken from Lins and Schanz [45] for an initial void ratio of 0.66. The optimization of the parameters of both hyperbolic and logarithmic retention models is given in Fig. 3. The fit is mostly based on capturing accurately the measured value of s_{AEV}, while the mathematical expression of the retention model influences the performance of the calibration at larger values of suction (for example, the logarithmic equation tends to capture more data points than the hyperbolic model). From a mechanical viewpoint, at least one isotropic or oedometric compression test is needed to determine stiffness parameters and critical breakage energy E_c. For this purpose, here we use an isotropic compression test reported by Daouadji et al. [44], who identified the first stress state at which the particle grading of Hostun sand begins to evolve upon hydrostatic conditions (Fig. 4a). The selected model parameters are collected in Table 1. It can be noted that, while L-E provides only a crude approximation of the measured compression response, pressure-dependent elasticity (PD-E) provides a more accurate prediction of the post-yielding response. Moreover, at the end of the isotropic compression test ($p = 15$ MPa), the predicted GSD shows good agreement with the measured GSD of the compressed specimen (Fig. 4b). The predicted suction-hardening is an outcome of such calibrated parameters, and is mathematically reflected by the factor $\chi_{HB}(S_r, B)$ appearing in the analytical expression of the comminution pressure. Substituting Eqs. (15) and (16) into Eqs. (10b) or (12b), the factor χ_{HB} can be plotted against S_r (Fig. 5a). Figure 5b illustrates the predicted hydrologic-induced hardening in terms of smeared suction ns. For this purpose, the retention curves in Eqs. (13) and (14) have been used. Only the drying branch of the retention response of Hostun sand has been considered for the sake of brevity. At large values of suction the predicted magnitude of the comminution pressure increases, thus causing the expansion of the predicted yielding domain. As pointed out in the previous sections, this result is a direct consequence of the fact that a larger value of the deformation energy is needed to cause crushing at low values of S_r. The pattern of the predicted suction hardening depends on the selected hyperelastic functions. For instance, Fig. 5 shows that PD-E tends to be associated with a suction-hardening effect larger than that obtained with L-E. As far as retention model is concerned, the hyperbolic retention curve predicts significant expansion at low values of S_r, while the logarithmic curve is associated with a weaker hardening effect (Fig. 5a). In addition, while the logarithmic model predicts the attainment of an asymptotic value for the size of the elastic domain at very large suctions, the hyperbolic model predicts a continuous increase of χ_{HB} upon drying (Fig. 5b). Although to the authors' knowledge there is no experimental valida-

Table 1 Model parameters for Hostun sand

Grainsize properties			Retention properties $e_0 = 0.66$		Mechanical properties $e_0 = 0.69$					
D_{50}	ϑ_M	ϑ_H	K_w for drying	K_w for wetting	p_{CR}	K	$\bar{K}$	ω	E_c for linear elasticity	E_c for P-D elasticity
mm			kPa	kPa	MPa	MPa		°	MPa	MPa
0.38	0.767	26.162	4	1	13.6	210	3,400	20	0.338	0.239

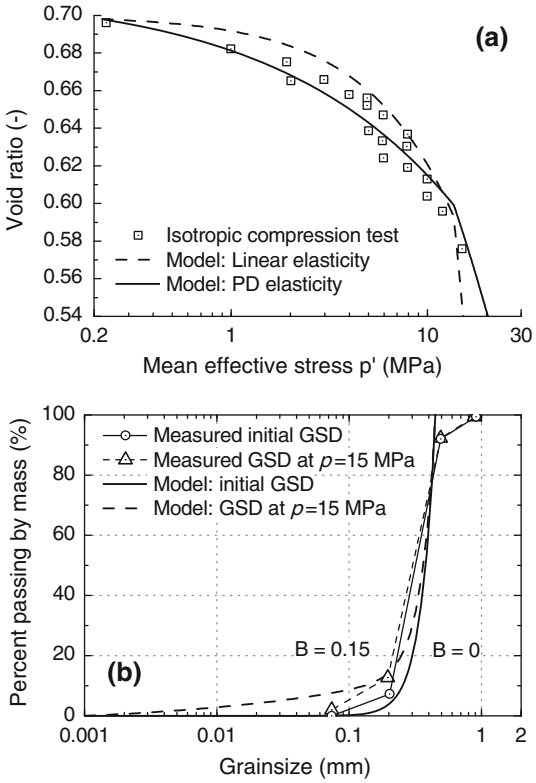

Fig. 4 Calibration of first yielding of Hostun sand based on **a** isotropic compression test causing particle breakage and **b** GSD before/after crushing (data after Daouadji et al.[44])

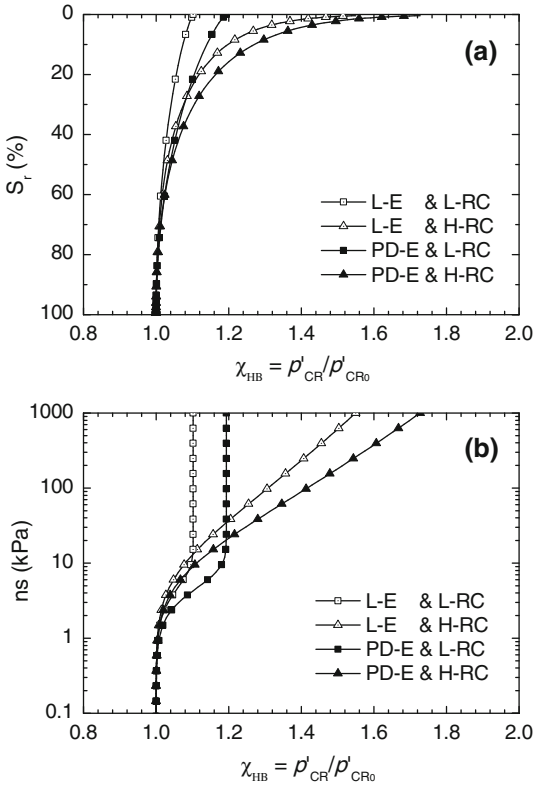

Fig. 5 Relation between yield stress and **a** degree of saturation **b** smeared suction

tion of such predictions, the simulated yielding domains have qualitative traits which resemble those reported in the literature for a range of unsaturated particulate media (e.g. [13], [21] and [46]).

Regardless of the selected model, the intensity of suction-hardening is controlled by a scalar quantity that depends on a specific set of model constants. Buscarnera and Einav [37] have named this quantity *capillary toughness number*, obtaining its expression by substituting the hydraulic potential (15) or (16) into the expressions (10b) and (12b)

$$\xi_{CT} = \vartheta_H \frac{K_w}{E_c} \tag{17}$$

This dimensionless factor reflects the effect of saturation condition on χ_{HB}, and it is dependent on model constants associated with the statistics of the particle grading (via ϑ_H), the suction air-entry value (via K_w) and the macroscopic energy threshold for breakage (via E_c). For the case of PD-E, the value here computed for Hostun sand is $\xi_{CT} = 0.44$. The importance of this parameter on the model predictions can be readily illustrated by considering a range of values for ξ_{CT} (Fig. 6). In particular, increasing values of ξ_{CT} can be associated with larger values of s_{AEV} (i.e., with increasing values of K_w) or, equivalently, with lower crushing strengths (i.e., with decreasing values of E_c). Figure 6 suggests that larger values of ξ_{CT} promote a stronger suction-hardening. As a result, ξ_{CT} can be viewed as a measure of the sensitivity of the yielding threshold to the state of saturation and, hence, as a measure of the intensity of coupled hydro-mechanical effects. The structure of ξ_{CT} reveals that such effect depends not only on the grain size distribution but also on the competition between crushing resistance and water-retention capa-

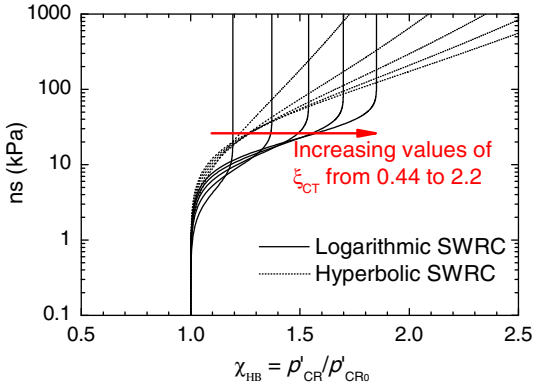

Fig. 6 Predicted yield curves in the $ns - \chi_{HB}$ plane for a range of values of capillary toughness number, ξ_{CT} (here increased up to a value five times larger than the initial calibration for Hostun sand, by magnifying its s_{AEV} via K_w)

bility. On one hand, ξ_{CT} is inversely proportional to E_c, suggesting that very high crushing resistance (and, hence, a limited possibility for internal energy dissipation) hinders the coupling effects. On the other hand, ξ_{CT} is proportional to K_w, suggesting that a pronounced water retention capacity (and, hence, stronger solid–fluid interactions) can amplify the coupling effects.

The role of particle breakage and degree of saturation on the evolution of the hydrostatic yielding stress of Hostun sand is illustrated in Fig. 7a. The figure shows that the predicted rate of clastic hardening changes with the assumed elastic model (with L-E associated with a sharper accumulation of breakage and PD-E characterized by a more gradual increase of the comminution pressure [40]). The value of the degree of saturation causes in all cases a shift of the $p' - B$ curves, predicting larger values of hydrostatic effective stress at the onset of comminution in dryer specimens. Figure 7b illustrates the effect of the capillary toughness number ξ_{CT} on the p'-B curves for PD-E and hyperbolic retention model (similar qualitative conclusions, however, could have been derived through any other combination of elastic and retention models). As expected, the comminution pressure becomes more sensitive to the saturation condition at larger values of ξ_{CT}. A comprehensive description of clastic yielding and suction-hardening can be obtained also for more general stress conditions, such as triaxial compression. Figure 8 shows three-dimensional plots of the yield surface on the p'-q-B space, as well as in the p'-q-S_r space. In the latter case, the suction-dependence of the predicted elastic domain closely resemble the classical loading collapse yield surfaces that are widely used in unsaturated soil models based on Cam-clay plasticity (e.g., [11,47] and [48]).

4 Grainsize dependence of hydro-mechanical coupling

The previous section has shown that microstructural considerations allow the prediction of changes in the mechanical and hydrologic properties of crushable media. In particular, hydro-mechanical couplings emerge spontaneously from the formulation, predicting suction-hardening in wet assemblies. Although the predicted couplings are an emanation of the scaling laws defined at particle scale, the macroscopic properties of the unbroken assembly come into play in defining such coupling terms (e.g., through the model constants K_w and E_c). Such macroscopic constants embedded in the energy potentials are calibrated via phenomenological considerations. These quantities are indirectly linked with the microstructural characteristics of the assembly and can be considered to be dependent on fundamental properties such as grain mineralogy, packing conditions, and initial grading.

Since the macroscopic constants of the unbroken assembly are affected by the characteristics of the initial particle grading, a phenomenological approach is pursued herein. More specifically, data from the literature are collected in the attempt to detect possible correlations between macroscopic model constants and geometric descriptors of the initial assembly (e.g., the mean grainsize, D_{50}). For example, Nakata et al. [1] investigated the high-pressure compression of quartzitic sands characterized by different particle grad-

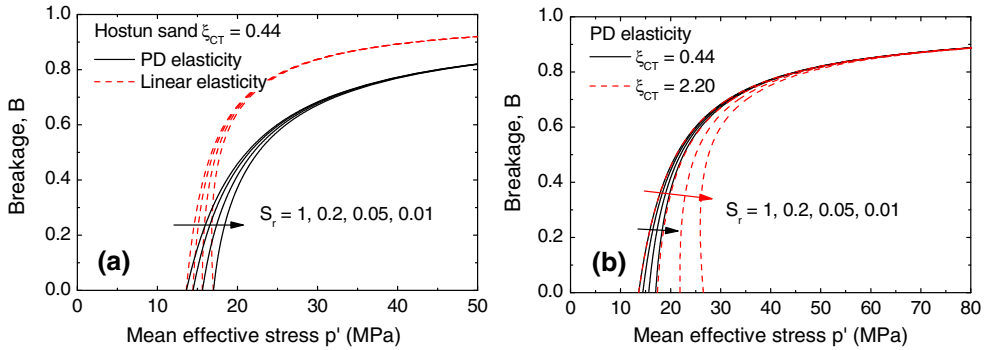

Fig. 7 **a** Evolution of the breakage index, B, under isotropic compression and **b** Effect of the degree of saturation on the $p' - B$ curves computed for different values of capillary toughness number

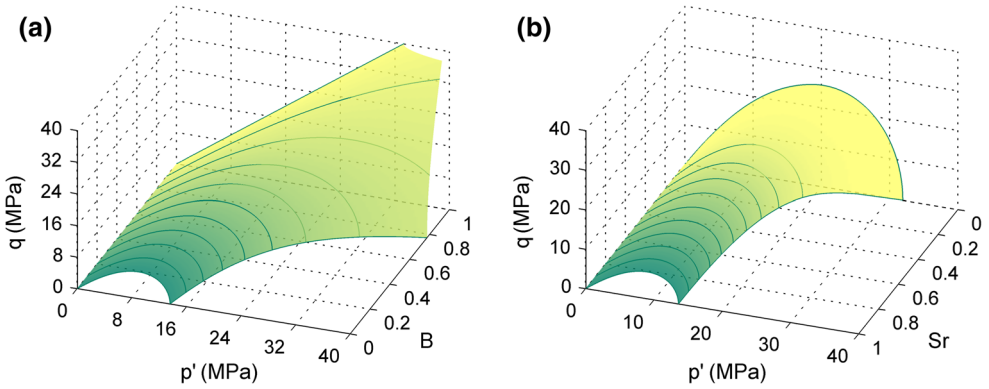

Fig. 8 Yield surfaces on **a** $p' - q - B$ space plotted for $S_r = 1$ and **b** $p' - q - S_r$ space plotted for $B = 0$

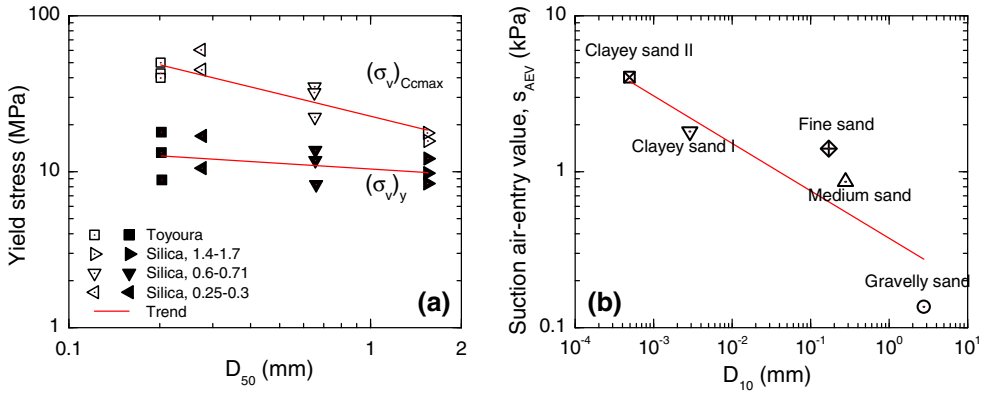

Fig. 9 **a** Effect of grain size on the vertical stress at yield $(\sigma_v)_y$ and at maximum compressibility $(\sigma_v)_{Ccmax}$ upon one-dimensional compression test (data after Nakata et al. [1]); **b** Effect of grain size on air-entry values (data after Yang et al.[9])

ings. Figure 9a presents the yield stress obtained from one-dimensional compression tests. This quantity is plotted as a function of the mean particle size D_{50}, thus inferring a decreasing trend of the yielding stress as the mean particle size increases. Also the hydraulic properties of granular assemblies are affected by the initial grain size distribution. Indeed, it has been extensively shown that capillary effects are more intense in presence of finer gradings [49,50], being the water retention curves of fine sands characterized by larger air-entry values (s_{AEV}) compared to coarser assemblies [9,51] (Fig. 9b). The reformulation of the Breakage Mechanics theory for unsaturated sands can provide guidance to incorporate the grainsize dependence of the macroscopic quantities and predict its implications on the model functions that control the hydro-mechanical coupling. In particular, since coupling effects are encapsulated in the capillary toughness number ξ_{CT}, the latter factor can be used to inspect the role of the grainsize characteristics on the intensity of suction-hardening. The magnitude of ξ_{CT} is indeed influenced by the model constants ϑ_H, K_w and E_c. While, the index ϑ_H is inherently associated with a given particle grading and can be determined in analytical form, the grainsize dependence of K_w and E_c must be assessed through experimental evidence. For this purpose, a dataset has been constructed by collecting literature data on water retention properties and compression response for a wide range of granular materials. To quantify the dependence of K_w on D_{50} a series of retention curves have been calibrated (for the sake of brevity, only the logarithmic model has been used to determine the value of K_w). Figure 10 illustrates an example of such a calibration procedure with reference to four sandy soils tested by Yang et al. [9] and characterized by a different mean grainsize. By extending this logic to a larger dataset, it has been possible to identify a correlation between K_w and D_{50} (the collected data is summarized in Table 2; Fig. 11). Although some scatter is observed because of factors that could not be sorted out from the data (e.g., packing conditions, grain angularity, mineralogy, etc.), the observed dependence between K_w and D_{50} can be accurately represented by a relation of the following form:

$$K_w = K_{w_{ref}} \left(\frac{D_{50}}{D_{ref}} \right)^{-a} \tag{18}$$

where $K_{w_{ref}}$ is assumed to be equal to 1 kPa, while D_{ref} and a are two fitting parameters. Such inverse trend is explained

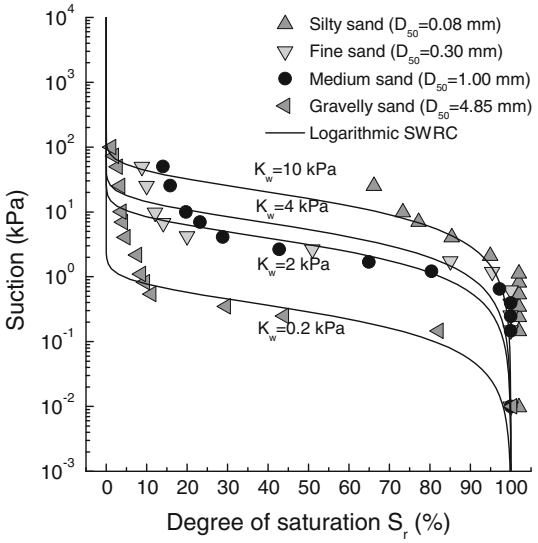

Fig. 10 Example of calibration of the SWRC constitutive parameters with respect to data collected for four sands having different GSD (data after Yang et al. [9]

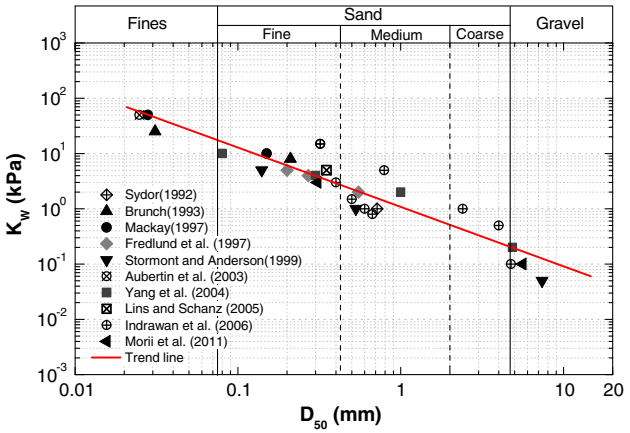

Fig. 11 Data set used to identify the grainsize dependence of the constitutive parameter K_w ($a = 1.074$ and $D_{ref} = 1.075$ mm have been used for the trend line in Eq. (18))

by the evidence that larger capillary pressures are required in finer soils to drain water from their pores ([49,50,52]). In fact, the observed slope $a = -1.074$ can again be justified by the capillary theory, by considering that the capillary pressure needed to drain a small cylindrical tube scales inversely with the tube diameter[32].

The conceptual origin of the dependence of E_c on D_{50} is less obvious than it is for the suction air-entry value. Indeed, as suggested by Einav [53], E_c can be considered as a property of the entire assembly (i.e., as a constant associated with a given mineralogy and particle angularity). Nevertheless, since no specific evaluation of the energy threshold E_c has been yet provided for a range of different mean particle diameters, here we use a phenomenological strategy similar to that used for K_w, in the attempt to quantify the possible correlation between E_c and the mean grainsize of the initial assembly, D_{50}. The experiments carried out by Nakata et al. [1] are a good starting point for this purpose. In fact, the data reported in Fig. 9a suggests that the yield stress depends on both initial void ratio and mean particle size. Figure 12a shows a series of one-dimensional compression tests performed on Toyoura sand samples characterized by the same GSD but different initial void ratios. The model constants that control the predicted compression response are calibrated on the basis of the compression test performed on a sample with $D_r = 43\,\%$ (Appendix B provides a strategy to estimate the yield stress $(\sigma_v)_{CR}$ and compute the associated value of E_c). The selected value of E_c (0.25 MPa) is then used to predict the compression response of the other two samples having different relative density (i.e., $D_r = 80$ and $98\,\%$). Only the initial stiffness prior to breakage is recalibrated for the new density conditions, while all the other parameters are left unaltered. The figure shows that this strategy produces a satisfactory prediction of the compression response. Such performance is no longer maintained when tests on sand samples with similar packing density but different mean grainsize are considered. This is illustrated in Fig. 12b with reference to one-dimensional compression tests on uniform silica sand. In this series of compression experiments the elastic properties remains substantially unchanged for values of D_{50} between 0.27 to 1.55 mm. By contrast, the yield stress decreases from 32.7 to 11 MPa, thus suggesting that E_c tends to decrease passing from fine-grained to coarse-grained materials. Such trend of reduction is corroborated by the calibration procedure, which suggests that an optimal fit of the measured compression response requires decreasing values of E_c.

Similar to the parameter K_w, a dataset can be constructed by calibrating the high-pressure compression of sands for a series of literature data. This dataset illustrates a clear correlation between the model parameter E_c and the average grainsize of a granular material, here summarized in Table 3 and Fig. 13. Such grainsize dependence of E_c can again be described via a power law:

$$E_c = E_{c_{ref}} \left(\frac{D_{50}}{D_{ref}} \right)^{-b} \tag{19}$$

where $E_{c_{ref}}$ is assumed to be equal to 1 MPa, while D_{ref} and b are two fitting parameters. A physical interpretation of this trend line can be obtained by considering the size dependence of the tensile strength of individual particles. As suggested by McDowell and Bolton [39], the aggregate yield stress under one-dimensional compression condition is associated with the tensile strength σ_f of the grains, which in turns scales inversely with the particle size according to a power law $\sigma_f \propto d^{-c}$ [54], where the exponent c of such a power law can in principle be estimated via linear elastic fracture

Table 2 Calibrated K_w values for different sands

Source	Material	D_{50} mm	Porosity	K_w kPa
[66]	Coarse sand	0.715	0.341	1
[55]	Beaver Creek sand	0.21	0.41	8
	Processed silt	0.031	0.35	25
[61]	London silt	0.028	0.382	50
	Ottawa sand	0.15	0.5	10
[57]	Sand(# 10,720)	0.55	0.41	2
	Loamy Sand (# 10,741)	0.2	0.39	5
	Sand (# 350)	0.27	0.33	4
[51]	Local silty sand	0.14	0.34	5
	Concrete sand	0.53	0.419	1
	Pea gravel	7.38	0.429	0.05
[52]	Tailings Sigma	0.025	0.347	50
[9]	Granitic residual soil	0.08	0.408	10
	Light grey beach sand	0.3	0.388	4
	Light brown construction sand	1	0.37	2
	Crushed granite	4.85	0.332	0.2
[45]	Hostun sand	0.35	0.357	5
[58]	Gravelly sand and residual soil mixture	4.75	0.32	0.1
		4	0.391	0.5
		2.4	0.319	1
		0.79	0.339	5
		0.32	0.368	15
	Medium sand and residual soil mixture	0.67	0.432	0.8
		0.6	0.411	1
		0.5	0.415	1.5
		0.4	0.416	3
		0.32	0.417	15
[62]	Fine sand	0.31	0.432	3
	Siliceous gravel	5.6	0.517	0.1

mechanics or through the Weibull's weakest link theory. It is therefore reasonable to argue that assembly comminution and grain fracture processes are intimately correlated. Nevertheless, establishing a direct theoretical connection of the grainsize dependence of the comminution pressure is a non-trivial task. As a result, for the sake of simplicity, here we evaluate the exponent of the power law in Eq. 19 through simple phenomenological considerations based on the collected dataset (Fig. 13).

These considerations suggest two possible scenarios for E_c, one in which this parameter is treated as a representative constant of the assembly (as originally argued by Einav [53]), and a second one in which E_c scales inversely with the average grainsize (as suggested by the dataset collected in Fig. 13). These scenarios must be combined with the inherent grainsize dependencies of ϑ_H and K_w to predict the role of the average grainsize on the intensity of hydro-mechanical coupling.

Figure 14 illustrates the implications on the predicted suction-dependence of clastic yielding due to the two possible scenarios for E_c. This is done by plotting the computed capillary toughness number ξ_{CT} against D_{50}. The dotted line illustrates the case in which E_c is assumed to be constant. In this scenario, the effect of the grainsize on the coupling terms derives only from capillary effects (i.e., from the grainsize dependence of ϑ_H and K_w). In this case, finer gradings are predicted to have larger values of ξ_{CT}, and hence a larger suction-hardening. A radically different conclusion is obtained by including the grainsize dependence of the crushing resistance. Indeed, if also E_c scales inversely with the mean grainsize (solid line in Fig. 14), the grainsize dependence of ξ_{CT} is inverted, suggesting that coarse gradings tends to have larger values of ξ_{CT} compared to finer soils. This finding implies that, for increasing values of average grainsize, the breakage energy threshold E_c decreases faster than the capillary effects ($\vartheta_H K_w$), thus originating a more

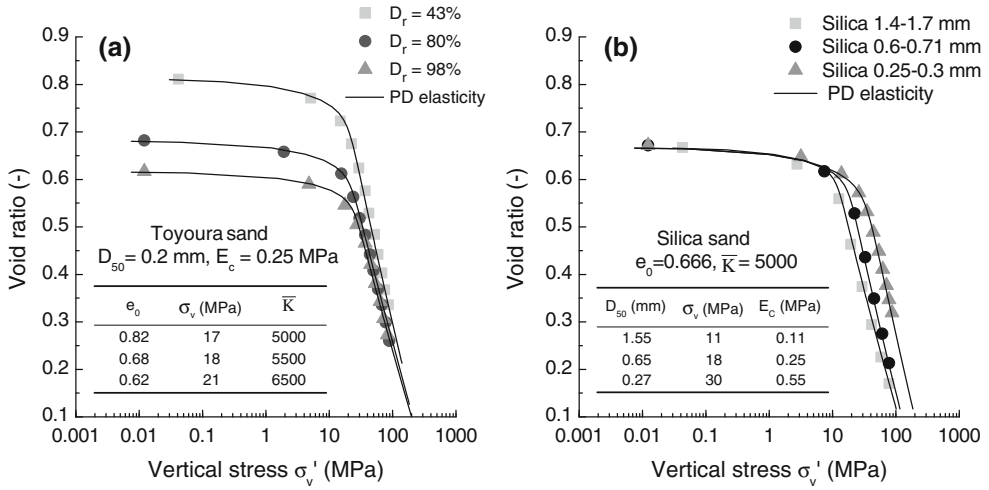

Fig. 12 Interpretation of high-pressure one-dimensional compression tests on **a** Toyoura sand at different values of relative density and **b** Silica sand with different values of mean particle size. (Data after Nakata et al. [1])

Table 3 Calibrated E_c values for different sands

Source	Material	D_{50} mm	e_0	$(\sigma_v)_{CR}$ MPa	ϑ_M	ω°	$\overline{K}$ MPa	E_c
[56]	Ground quartz	0.08	0.84	5.5	0.737	10	2,600	0.51
[65]	Ottawa sand, quartz, well rounded	0.6	0.59	25	0.773	69	10,000	0.30
		0.48	0.49	35	0.77	69	12,000	0.36
[59]	Crushed granitic gravelly sand	4.85	0.71	3.3*	0.789	10	2,000	0.03
[64]	Ottawa sand	0.14	0.66	45	0.751	45	6,000	0.70
		0.14	0.82	29	0.751	30	3,500	0.70
[44]	Hostun sand	0.38	0.69	13.6*	0.767	20	3,400	0.24
[1]	Silica sand, quartz	1.55	0.67	11	0.781	67	5,000	0.11
		0.65	0.67	18	0.774	65	5,000	0.25
		0.27	0.67	30	0.762	60	5,000	0.55
	Toyoura sand, rounded quartz	0.2	0.82	17	0.757	62	5,000	0.25
[63]	Silica, angular quartz	0.75	0.43	20	0.775	51	5,000	0.22
		0.75	0.67	10	0.775	34	2,400	0.18
[15]	Pancrudo rockfill	24.2	0.55	0.7	0.795	25	1,000	0.01
[4]	Mono-quartz sand	0.1	0.75	20.8	0.743	69	2,500	0.50
		0.19	0.74	21.5	0.756	38	4,000	0.34
		0.33	0.83	14	0.765	69	2,200	0.33
		0.71	0.73	9.8	0.775	25	3,000	0.14
		0.85	0.75	7.9	0.776	40	3,000	0.10
		1.51	0.75	6.6	0.781	50	3,000	0.08
		2.3	0.75	1.2	0.784	55	3,000	0.07
[60]	Melito rockfill, schist, angular	12.06	0.59	0.7	0.793	25	1,000	0.01

* indicates isotropic compression tests, for which $(\sigma_v)_{CR}$ is corresponding to p_{CR}

pronounced water-sensitivity of coarser assemblies. In other words, although the absolute value of both the energy threshold for comminution and the additional energy barrier due to capillarity are predicted to be deteriorated by particle size effects, the power laws used to capture the grainsize dependence of the model constants suggest that the relative effect of solid–fluid energy interactions tends to be stronger at the macroscale in presence of larger and more fragile particles. The effect of the grainsize can be further inspected by plotting the predicted suction hardening curves for different values of D_{50} (corresponding to different values of ξ_{CT}, as shown in Fig. 15). Three values of mean grainsize have been considered, labeled as fine, medium and coarse sand, respectively. For the three cases, the predicted value of the hardening fac-

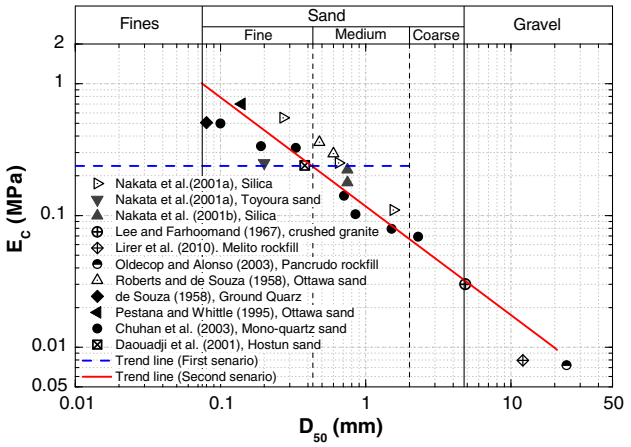

Fig. 13 Data set used to identify the grainsize dependence of E_c. Two scenarios have been considered, namely constant E_c (E_c=0.24 MPa) and grainsize dependent E_c [with $b = 0.826$ and $D_{ref} = 0.075$ mm for the trend line in Eq. (19)]. Parameters obtained through a calibration procedure based on the use of an initial Poisson's ratio ν of 0.25 and a stress ratio at frictional failure M of 1.3.

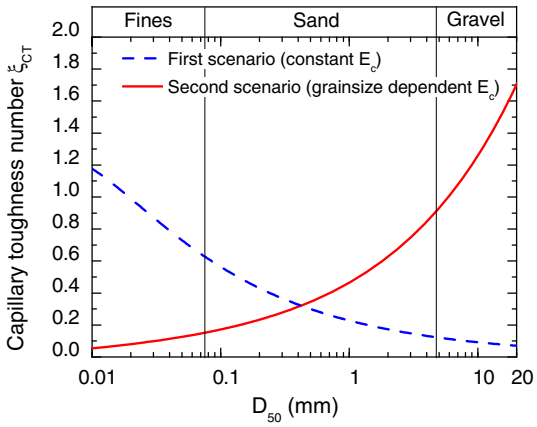

Fig. 14 Predicted dependence of the capillary toughness number, ξ_{CT}, on the average grainsize, D_{50}

tor ξ_{CT} has been computed, inspecting the two above mentioned scenarios for E_c. In accordance with Fig. 14, the computed suction-hardening curves suggest a grainsize dependence of the magnitude of the expansion/contraction of the elastic domain due to changes in suction and/or degree of saturation.

5 Conclusions

The paper has addressed the coupling between mechanical and hydrologic processes in crushable media. The main goal of the study has been to understand how particle-scale processes and grainsize characteristics control the dependence of grain crushing on suction and degree of saturation.

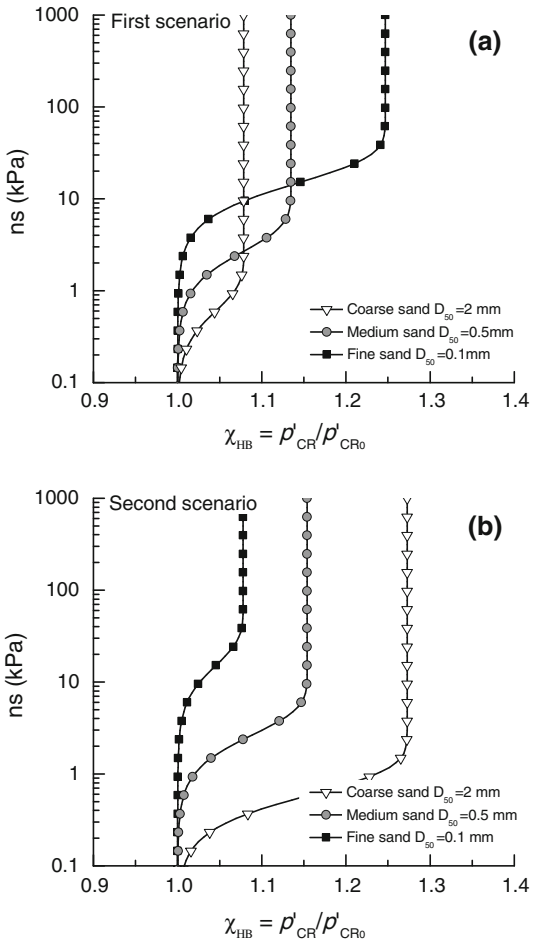

Fig. 15 Normalized suction-hardening curves predicted for three types of sands by assuming **a** constant $E_c = 0.24$ MPa and **b** grainsize dependent E_c as in Eq. (19). Only the results obtained through logarithmic retention model are displayed, determining the value of the parameter K_w via Eq. (18).

For this purpose, we have adopted a continuum framework inspired by the linkage of breakage mechanics and capillary theory. First, we have calibrated the model parameters for an extensively studied granular material (Hostun sand), exploring the effect of specific choices for the hydro-mechanical energy potentials (i.e., elastic potentials and water retention models). This strategy has allowed us to predict a possible influence of elastic and water-retention properties on clastic hardening and suction-induced hardening. The analyses have pointed out that the intensity of coupling is controlled by a dimensionless factor (here referred to as capillary toughness number, ξ_{CT}) whose value is controlled by the statistics of particle grading (i.e., by a grading index, ϑ_H), as well as by the model constants that control the suction air-entry value (i.e., K_w) and the energy input for initiating particle crushing (i.e., E_c). The grainsize dependence of this non-dimensional number has been investigated by collecting literature data on water-retention

properties and high-pressure compression of granular media. Two datasets have been constructed for the model parameters K_w and E_c. Given the macroscopic connotation of the hydro-mechanical properties associated with them, the two datasets have emphasized a correlation between the two model constants and a descriptor of the initial assembly (i.e., the mean grainsize D_{50}). Such relations have predicted two contrasting scenarios for the coupling between degree of saturation and yielding. In the first scenario, K_w (and, hence, the suction air-entry value) scales inversely with the average grainsize, while the energy input initiating comminution (i.e., E_c) is independent of the grainsize. Given the definition of ξ_{CT}, this assumption implies that changes in the degree of saturation play a more intense role in finer gradings compared to coarse-grained systems. Conversely, if we assume that also E_c scales inversely with the mean grainsize (as indicated by the collected data), the effect of the degree of saturation is predicted to be stronger in coarser assemblies. In other words, the deterioration of the yielding stress due to grainsize scaling effects is predicted to exacerbate water-sensitivity of a partially saturated assembly made of crushable grains. This result provides an interpretation for the evidence that solid–fluid interactions have a noticeable role in assemblies made of coarse particles (e.g., gravels), while they tend to play little or no role in granular materials characterized by a finer grading (e.g., sands). While the particle-scale assumptions that have inspired these results make reference to a specific class of particulate media (i.e., sands) and cannot be directly applied to a broader set of unsaturated soils (e.g., clays, silts or rockfill), they confirm that multi-scale models based on microscopic physical considerations represent a promising approach to incorporate microstructural descriptors and can disclose effects which would not be immediately apparent from pure macroscopic modeling.

Acknowledgments This work has been initiated under a booster fund granted by the Institute of Sustainability and Energy at Northwestern (ISEN) and has been partially supported by grant No. CMMI-1351534 awarded by the Geomechanics and Geomaterials program of the U.S. National Science Foundation.

Appendix A: Grading indices for uniform grainsize distributions

If the probability for a given particle of size x to exist within the interval (D_m, D_M) is assumed to be constant:

$$p(x) = \frac{1}{D_M - D_m} \tag{20}$$

it is possible to show that the corresponding cumulative grain size distribution by number is given by:

$$F(x) = \int_{D_m}^{x} p(y)dy = \frac{x - D_m}{D_M - D_m} \tag{21}$$

By further assuming that the mass of each particle x is proportional to x^3, the cumulative GSD by mass is can be derived as

$$F^*(x) = \frac{\int_{D_m}^{x} p(y)y^3 dy}{\int_{D_m}^{D_M} p(y)y^3 dy} = \frac{x^4 - {D_m}^4}{{D_M}^4 - {D_m}^4} \tag{22}$$

Then the corresponding probability density function by mass can be derived as

$$g(x) = \frac{dF^*(x)}{dx} = \frac{4x^3}{{D_M}^4 - {D_m}^4} \tag{23}$$

Equation (22) shows good agreement with the initial grading of the commercial sands such as Hostun sand, as shown in Fig. 2. As far as the probability density function of the GSD at complete breakage, it is possible to use the expression suggested by Einav (2007a):

$$g_u(x) = \frac{(3-\alpha)x^{2-\alpha}}{{D_M}^{3-\alpha} - {D_m}^{3-\alpha}} \tag{24}$$

where α is the fractal dimension (usually set to be 2.7). It is interesting to note that Eq. (23) is a particular case of equation Eq. (24), obtained by setting α equal to -1.

The grading indices associated with the previously defined GSD curves can be expressed as:

$$\begin{aligned}\vartheta_M &= 1 - \frac{\int_{D_m}^{D_M} g_u(x)\,x^2 dx}{\int_{D_m}^{D_M} g_0(x)\,x^2 dx} \\ &= 1 - \frac{3}{2}\left(\frac{3-\alpha}{5-\alpha}\right)\left(\frac{{D_M}^4 - {D_m}^4}{{D_M}^6 - {D_m}^6}\right)\left(\frac{{D_M}^{5-\alpha} - {D_m}^{5-\alpha}}{{D_M}^{3-\alpha} - {D_m}^{3-\alpha}}\right)\end{aligned} \tag{25a}$$

$$\begin{aligned}\vartheta_H &= \frac{\int_{D_m}^{D_M} g_u(x)\,x^{-1} dx}{\int_{D_m}^{D_M} g_0(x)\,x^{-1} dx} - 1 \\ &= \frac{3}{4}\left(\frac{3-\alpha}{2-\alpha}\right)\left(\frac{{D_M}^4 - {D_m}^4}{{D_M}^3 - {D_m}^3}\right)\left(\frac{{D_M}^{2-\alpha} - {D_m}^{2-\alpha}}{{D_M}^{3-\alpha} - {D_m}^{3-\alpha}}\right) - 1\end{aligned} \tag{25b}$$

Both indices can be determined by specifing the maximum and minimum particle size (the latter being usually assumed to be 1 mm). In particular, by using Eq. (22) it is possible to express the maximum grainsize D_M as a function of the mean grainsize D_{50}, as follows:

$$D_M = \left(2{D_{50}}^4 - {D_m}^4\right)^{1/4} \tag{26}$$

As a result, the two grading indices given in Eq. (25) can be plotted as a function of D_{50} (1).

Appendix B: Yield stress upon one-dimensional compression

The vertical stress associated with the onset of comminution upon one-dimensional compression, $\left(\sigma_V'\right)_{CR_0}$ can be computed by enforcing the yielding condition for a K_0 compression path. In this case, the stress path implies that $q = 3(1-K_0)\,p'/(1+2K_0)$ or $\sigma_v{}' = 3p'/(1+2K_0)$. Substituting these relations in Eq. (6), the yield stress for a saturated linear elastic medium is given by:

$$\left(\sigma_V{}'\right)_{CR_0} = \frac{3}{1+2K_0}\sqrt{\frac{2E_c\left(1-\frac{\eta_{K0}{}^2}{M^2}\right)}{\vartheta_M\left(\frac{1}{K}+\frac{\eta_{K0}{}^2}{3G}\right)}} \tag{27}$$

where $\eta_{K0} = 3(1-K_0)\Big/(1+2K_0)$. In the case of pressure-dependent elasticity, the yield function can be obtained by combining Eqs. (5),(6) and (11):

$$\frac{\vartheta_M(1-B)^2}{E_c}\left[\frac{p_r}{\bar{K}(2-m)}\frac{\zeta(p',q)^{2-m}}{(1-\vartheta_M B)^{2-m}}+\frac{q^2}{6p_r\bar{G}}\frac{\zeta(p',q)^{-m}}{(1-\vartheta_M B)^2}\right] + \left(\frac{q}{Mp'}\right)^2 \leq 1+\frac{\vartheta_H}{E_c}\psi_r^H(S_r)(1-B)^2 \tag{28}$$

where

$$\zeta(p',q) = \frac{p'}{2p_r}+\sqrt{\left(\frac{p'}{2p_r}\right)^2-\frac{\bar{K}m}{6\bar{G}}\left(\frac{q}{p_r}\right)^2} \tag{29}$$

The $\left(\sigma_V'\right)_{CR_0}$ for pressure-dependent elasticity can again be obtained by assuming a K_0 compression path, as follows:

$$\left(\sigma_V{}'\right)_{CR_0} = \frac{3}{1+2K_0}\left[\frac{E_c\left(1-\frac{\eta_{K0}{}^2}{M^2}\right)}{\vartheta_M\left(\frac{p_r{\zeta_{K0}}^{2-m}}{\bar{K}(2-m)}+\frac{{\eta_{K0}}^2{\zeta_{K0}}^{-m}}{6p_r\bar{G}}\right)}\right]^{\frac{1}{2-m}} \tag{30}$$

where

$$\zeta_{K0} = \frac{\zeta(p',q)}{p'} = \frac{1}{2p_r}+\sqrt{\left(\frac{1}{2p_r}\right)^2-\frac{\bar{K}m{\eta_{K0}}^2}{6\bar{G}{p_r}^2}} \tag{31}$$

The above relations have been used to identify the optimal values of E_c allowing the mathematical capture of numerous compression experiments available in the literature (Fig. 13).

References

1. Nakata, Y., Kato, Y., Hyodo, M., Hyde, A.F., Murata, H.: One-dimensional compression behaviour of uniformly graded sand related to single particle crushing strength. Soils Found. **41**(2), 39–51 (2001)
2. Lade, P.V., Yamamuro, J.A., Bopp, P.A.: Significance of particle crushing in granular materials. J. Geotech. Eng. **122**(4), 309–316 (1996)
3. Hardin, B.O.: Crushing of soil particles. J. Geotech. Eng. **111**(10), 1177–1192 (1985)
4. Chuhan, F.A., Kjeldstad, A., Bjørlykke, K., Høeg, K.: Experimental compression of loose sands: relevance to porosity reduction during burial in sedimentary basins. Can. Geotech. J. **40**(5), 995–1011 (2003)
5. Zoback, M.D., Byerlee, J.D.: Effect of high-pressure deformation on permeability of ottawa sand. AAPG Bull. **60**(9), 1531–1542 (1976)
6. Papamichos, E., Vardoulakis, I., Ouadfel, H.: Permeability reduction due to grain crushing around a perforation. Int. J. Rock Mech. Min. Sci. abstr. **30**, 1223–1229 (1993)
7. DeJong, J.T., Christoph, G.G.: Influence of particle properties and initial specimen state on one-dimensional compression and hydraulic conductivity. J. Geotech. Geoenviron. Eng. **135**(3), 449–454 (2009)
8. Arya, L.M., Paris, J.F.: A physicoempirical model to predict the soil moisture characteristic from particle-size distribution and bulk density data. Soil Sci. Soc. Am. J. **45**(6), 1023–1030 (1981)
9. Yang, H., Rahardjo, H., Leong, E.C., Fredlund, D.G.: Factors affecting drying and wetting soil–water characteristic curves of sandy soils. Can. Geotech. J. **41**(5), 908–920 (2004)
10. Jamei, M., Guiras, H., Chtourou, Y., Kallel, A., Romero, E., Georgopoulos, I.: Water retention properties of perlite as a material with crushable soft particles. Eng. Geol. **122**(3), 261–271 (2011)
11. Alonso, E.E., Gens, A., Josa, A.: A constitutive model for partially saturated soils. Géotechnique **40**(3), 405–430 (1990)
12. Gallipoli, D., Gens, A., Sharma, R., Vaunat, J.: An elasto-plastic model for unsaturated soil incorporating the effects of suction and degree of saturation on mechanical behaviour. Géotechnique **53**(1), 123–136 (2003)
13. Gens, A.: Soil-environment interactions in geotechnical engineering. Géotechnique **60**(1), 3–74 (2010)
14. Oldecop, L.A., Alonso, E.E.: A model for rockfill compressibility. Géotechnique **51**(2), 127–139 (2001)
15. Oldecop, L.A., Alonso, E.E.: Suction effects on rockfill compressibility. Géotechnique **2**, 289–292 (2003)
16. Alonso, E.E., Olivella, S., Hugas, J.: Modelling the behaviour of an earth and rockfill dam during construction and impoundment. Unsat. Soils: Numer. and Theor. Approach., pp. 269–287. (2005)
17. Heath, A.C., Pestana, J.M., Harvey, J.T., Bejerano, M.O.: Normalizing behavior of unsaturated granular pavement materials. J. Geotech. Geoenviron. Eng. **130**(9), 896–904 (2004)
18. Frey, R.G., Halloran, J.: Compaction behavior of spray-dried alumina. J. Am. Ceram. Soc. **67**(3), 199–203 (1984)
19. Nieuwmeyer, F.J., van der Voort Maarschalk, K., Vromans, H.: Granule breakage during drying processes. Int. J. Pharm. **329**(1), 81–87 (2007)
20. Maatouk, A., Leroueil, S., La Rochelle, P.: Yielding and critical state of a collapsible unsaturated silty soil. Géotechnique **45**(3), 465–477 (1995)
21. Cui, Y., Delage, P.: Yielding and plastic behaviour of an unsaturated compacted silt. Géotechnique **46**(2), 291–311 (1996)
22. Romero, E., Della Vecchia, G.: An insight into the water retention properties of compacted clayey soils. Géotechnique **61**(4), 313–328 (2011)

23. Oldecop, L.A., Alonso, E.E.: Theoretical investigation of the time-dependent behaviour of rockfill. Géotechnique **57**(3), 289–301 (2007)
24. Chávez, C., Alonso, E.E.: A constitutive model for crushed granular aggregates which includes suction effects. Soils Found. **43**(4), 215–227 (2003)
25. Soulie, F., Cherblanc, F., El Youssoufi, M.S., Saix, C.: Influence of liquid bridges on the mechanical behaviour of polydisperse granular materials. Int. J. Numer. Anal. Methods Geomech. **30**(3), 213–228 (2006)
26. Richefeu, V., El Youssoufi, M.S., Radjai, F.: Shear strength properties of wet granular materials. Phys. Rev. E **73**(5), 051,304 (2006)
27. Alonso, E.E. and Romero, E.: Collapse behaviour of sand. Proc. Of the 2nd Asian Conf. on Unsat. Soils (2003)
28. Houlsby, G.: The work input to an unsaturated granular material. Géotechnique **47**(1), 193–196 (1997)
29. Gili, J.A., Alonso, E.E.: Microstructural deformation mechanisms of unsaturated granular soils. Int. J. Numer. Anal. Methods Geomech. **26**(5), 433–468 (2002)
30. Li, X.S.: Effective stress in unsaturated soil: a microstructural analysis. Géotechnique **53**(2), 273–277 (2003)
31. Scholtès, L., Chareyre, B., Nicot, F., Darve, F.: Micromechanics of granular materials with capillary effects. Int. J. Eng. Sci. **47**(1), 64–75 (2009)
32. Fisher, R.: On the capillary forces in an ideal soil; correction of formulae given by wb haines. J. Agric. Sci. **16**(03), 492–505 (1926)
33. Oda, M., Iwashita, K.: Mechanics of granular materials: an introduction. A.A.Balkema, Rotterdam (1999)
34. Einav, I.: Breakage mechanicspart I: theory. J. Mech. Phys. Solids **55**(6), 1274–1297 (2007)
35. Einav, I.: Breakage mechanicsł part II: modelling granular materials. J. Mech. Phys. Solids **55**(6), 1298–1320 (2007)
36. Einav, I.: Fracture propagation in brittle granular matter. Proc. Roy. Soc. Lond. Ser. A **463**(2087), 3021–3035 (2007)
37. Buscarnera, G., Einav, I.: The yielding of brittle unsaturated granular soils. Géotechnique **62**(2), 147–160 (2012)
38. Collins, I.F., Houlsby, G.T.: Application of thermomechanical principles to the modelling of geotechnical materials. Proc. Roy. Soc. Lond. Ser. A **453**(1964), 1975–2001 (1997)
39. McDowell, G.R., Bolton, M.D.: On the micromechanics of crushable aggregates. Géotechnique **48**(5), 667–679 (1998)
40. Nguyen, G.D., Einav, I.: The energetics of cataclasis based on breakage mechanics. Pure Appl. Geophys. **166**(10–11), 1693–1724 (2009)
41. Einav, I., Puzrin, A.: Pressure-dependent elasticity and energy conservation in elastoplastic models for soils. J. Geotech. Geoenviron. Eng. **130**(1), 81–92 (2004)
42. Lloret, A., Alonso, E.E.: Consolidation of unsaturated soils including swelling and collapse behaviour. Géotechnique **30**(4), 449–477 (1980)
43. Flavigny, E., Desrues, J., Palayer, B.: Note technique-le sable d'hostun "rf". Revue française de géotechnique **53** (1990)
44. Daouadji, A., Hicher, P.Y., Rahma, A.: An elastoplastic model for granular materials taking into account grain breakage. Eur. J. Mech. A-Solid **20**(1), 113–137 (2001)
45. Lins, Y., Schanz, T.: Determination of hydro-mechanical properties of sand. Unsat. Soils: Exp. Studies, pp. 15–32. (2005)
46. Lloret, A., Villar, M.V., Snchez, M., Gens, A., Pintado, X., Alonso, E.E.: Mechanical behaviour of heavily compacted bentonite under high suction changes. Géotechnique **53**(1), 27–40 (2003)
47. Loret, B., Khalili, N.: An effective stress elastic–plastic model for unsaturated porous media. Mech. Mater. **34**(2), 97–116 (2002)
48. Gens, A., Sánchez, M., Sheng, D.: On constitutive modelling of unsaturated soils. Acta Geotech. **1**(3), 137–147 (2006)
49. Terzaghi, K., Peck, R., Mesri, G.: Soil Mechanics in Engineering Practice. Wiley, New York (1996)
50. Kovács, G.: Seepage Hydraulics. Elsevier, Amsterdam (1981)
51. Stormont, J.C., Anderson, C.E.: Capillary barrier effect from underlying coarser soil layer. J. Geotech. Geoenviron. Eng. **125**(8), 641–648 (1999)
52. Aubertin, M., Mbonimpa, M., Bussière, B., Chapuis, R.: A model to predict the water retention curve from basic geotechnical properties. Can. Geotech. J. **40**(6), 1104–1122 (2003)
53. Einav, I.: Fracture propagation in brittle granular matter. Proc. Roy. Soc. Lond. Ser. A **463**(2007), 3021–3035 (2007)
54. Lee, D.M.: The angles of friction of granular fills. Ph.D. thesis, Cambridge University (1992)
55. Bruch, P.: A laboratory study of evaporative fluxes in homogeneous and layered soils. M.sc. thesis, University of Sas- katchewan, Saskatoon, Saskatchewan (1993)
56. De Souza, J.: Compressibility of quartz sand at high pressure. M.sc. thesis, Massachusetts Institute of Technology, Cambridge, Mass. (1958)
57. Fredlund, M.D., Fredlund, D.G., Wilson, G.: Prediction of the soil-water characteristic curve from grain-size distribution and volume–mass properties. In: Proc., 3rd Brazilian Symp. on Unsat. Soils, vol. 1, pp. 13–23. Rio de Janeiro (1997)
58. Indrawan, I., Rahardjo, H., Leong, E.C.: Effects of coarse-grained materials on properties of residual soil. Eng. Geol. **82**(3), 154–164 (2006)
59. Lee, K.L., Farhoomand, I.: Compressibility and crushing of granular soil in anisotropic triaxial compression. Can. Geotech. J. **4**(1), 68–86 (1967)
60. Lirer, S., Flora, A., Nicotera, M.: Some remarks on the coefficient of earth pressure at rest in compacted sandy gravel. Acta Geotech. **6**(1), 1–12 (2011)
61. MacKay, P.L.: Evaluation of oxygen diffusion in unsaturated soils. M.sc. thesis, The University of Western Ontario (1997)
62. Morii, T., Inoue, M., Kadoguchi, R.: Effective water harvesting using capillary barrier of unsaturated soils. Unsat. Soils: Theor. Pract. pp. 857–860 (2011)
63. Nakata, Y., Hyodo, M., Hyde, A.F., Kato, Y., Murata, H.: Microscopic particle crushing of sand subjected to high pressure one-dimensional compression. Soils Found. **41**(1), 69–82 (2001)
64. Pestana, J.M., Whittle, A.: Compression model for cohesionless soils. Géotechnique **45**(4), 611–631 (1995)
65. Roberts, J.E., De Souza, J.M.: The compressibility of sands. P. Am. Soc. Test Mater. **58**(4), 1269–1272 (1958)
66. Sydor, R.: Engineered mine tailings cover: verification of drainage behaviour and investigations of design. M.sc. thesis, University of Waaterloo (1992)